Article:

Sonnenwald, F. orcid.org/0000-0002-2822-0406, Mark, O., Stovin, V. orcid.org/0000-0001-9444-5251 et al. (1 more author) (2021) Predicting manhole mixing using a compartmental model. Journal of Hydraulic Engineering, 147 (12). ISSN 0733-9429

https://doi.org/10.1061/(ASCE)HY.1943-7900.0001951

Predicting manhole mixing using a compartmental model

Fred Sonnenwald[1], Ole Mark[2], Virginia Stovin[3], Ian Guymer[4]

[1]Research Associate, Department of Civil & Structural Engineering, The University of Sheffield, Mappin Street, Sheffield, S1 3JD, United Kingdom

[2]Head of Innovation, Krüger A/S, 2860 Søborg, Denmark

[3]Professor of Green Infrastructure for Stormwater Management, Department of Civil & Structural Engineering, The University of Sheffield, Mappin Street, Sheffield, S1 3JD, United Kingdom

[4]Professor of Civil Engineering, Department of Civil & Structural Engineering, The University of Sheffield, Mappin Street, Sheffield, S1 3JD, United Kingdom

ABSTRACT

Manholes in combined sewers may become surcharged during storm events, resulting in complex mixing conditions. Although manhole hydrodynamics are reasonably well understood, predicting mixing across a surcharged manhole remains a challenge. An analytical compartmental mixing model for manholes, based on jet theory, has been further developed and applied to generate cumulative residence time distributions (CRTDs), which describe mixing. The modelled CRTDs were compared with the experimentally derived CRTDs of over 850 manhole configurations to evaluate how well the new compartmental model represents physical processes. The model underpredicts short-circuiting in manholes with manhole diameter to pipe diameter ratios greater than 4.4 and consequently overestimates mixing. Otherwise, the modelled CRTDs show good agreement with the experimental CRTDs. The new compartmental model represents key manhole hydrodynamics that are not represented in current software modelling packages, which assume manholes are instantaneously well-mixed. The compartmental model provides good predictions of the experimental downstream concentration profiles, although with reduced peak concentrations in those manhole

configurations where short-circuiting is not well-predicted. Despite this, the compartmental model still predicts concentrations downstream of a manhole in closer agreement with the recorded data than the complete instantaneously well-mixed assumption. As an analytical model requiring no inputs other than manhole geometry, the new compartmental model applies to a wide range of manhole configurations, is robust, and is useful for predicting manhole mixing in practical applications.

Keywords: Water quality, manholes, mixing, short-circuiting, sewers, contaminant transport, travel time, hydraulic structures, residence time, pollutants

INTRODUCTION

Combined sewer networks convey waste water to treatment. Manholes are placed in sewer networks at regular intervals, at junctions, and changes in direction for inspection and maintenance. During storm events, high flows may lead to manholes becoming surcharged, where the water level exceeds the inlet pipe soffit, which in turn could result in combined sewer overflows into receiving waters, or, in extreme cases, flooding (Butler et al., 2018).

At present, there is a focus on improving water quality within receiving waters. For example, the Water Framework Directive (European Union Commission, 2000) calls for action to achieve good qualitative and quantitative ecological status of all water bodies. Water quality processes within combined sewer networks are relevant to understanding and reducing the pollutant load on receiving waters. Software modelling packages such as SWMM (Rossman, 2015), InfoWorks ICM (Innovyze Inc., 2019), and MIKE URBAN+ (formerly MOUSE) (DHI A/S, 2019) are commonly used to evaluate both water quantity and water quality in sewer networks (Obropta and Kardos, 2007).

Significant efforts have been devoted to understanding the hydraulics of sewer networks. Less effort has been dedicated to understanding mixing processes within sewer networks. SWMM, InfoWorks ICM, and MIKE URBAN+ all assume inflow into manholes is instantaneously well-mixed with the water volume. However, Stovin et al. (2013) has shown that, depending on both the surcharge level within the manhole and the manhole geometry, more complex mixing conditions occur, and, in these instances, a well-mixed assumption may be invalid and subsequently lead to erroneous estimations of pollutant concentrations in sewers. This paper presents an improved method of predicting mixing due to manholes of different geometries over a range of surcharge and discharge conditions, suitable for inclusion into software packages.

Manholes come in a variety of geometries, including t-shaped, rectangular, and circular (Butler et al., 2018). Manholes may be shallow or deep, with access shafts, and may also have the inlet and outlet at different elevations (stepped). In addition to multiple inlets, differing pipe diameters, or an angle between inlet and outlet, manholes often have a dry weather channel and benching, and in many cases, the pipe may be offset from the manhole centerline. A simple manhole geometry of a circular unbenched straight-through manhole has been most used to study mixing, e.g., Guymer and O'Brien, (2000) and Guymer et al. (2005). These studies applied the Advection-Dispersion Equation (ADE) and Aggregated Dead Zone (ADZ) model (Rutherford, 1994) to investigate mixing within surcharged manholes. Both studies showed the ADE and ADZ model to predict mixing poorly and failed to provide a generalized means of predicting model parameters.

Mixing within manholes is a non-Gaussian process that is dependent on surcharge depth and manhole diameter to inlet pipe diameter ratio (D_m/D_p) (Guymer et al., 2005; Guymer and Stovin, 2011; Stovin et al., 2013). For straight $D_m/D_p > 4.4$ manholes, a threshold surcharge depth (S') exists. When surcharge depth S is below-threshold, $S < S'$, mixing is complete, while above-threshold, $S > S'$, short-circuiting occurs. For straight $D_m/D_p \leq 4.4$ manholes, there is no threshold and only short-circuiting flow conditions occur, regardless of surcharge depth. Fig. 1 shows laser-induced fluorescence (LIF) images of dye traces in a model manhole. Fig. 1a shows below-threshold flow, which expands throughout the entire manhole volume producing well-mixed conditions. Fig. 1b shows above-threshold flow, where a jet of dye short-circuits from the inlet to the outlet. Dye that does not exit directly recirculates in the manhole volume, which acts as a dead zone. In circular unbenched straight-through manholes, Stovin et al. (2010) reported the threshold at $S' = 0.258D_m$ for $D_m/D_p > 4.4$. However, there is evidence that this threshold value is different for more complex manhole geometries, for example in 30-90° angled $D_m/D_p = 4.4$ manholes, Sonnenwald (2014) reported $S' \approx 0.7D_m$.

There is a link between mixing and energy losses, as both result from the same hydrodynamic processes; higher energy losses tend to be associated with higher levels of mixing (Guymer et al., 2005). Below-threshold, head-loss coefficients increase with surcharge depth, showing more energy is dissipated by the chaotic well-mixed flow field. Above-threshold head loss coefficients reduce and remain constant, reflecting the more ordered short-circuiting/recirculating flow field (Arao and Kusada, 1999; Stovin et al., 2013). Using head loss data, Beg et al. (2019) reported $S' = 0.33D_m$ in 15-30° angled $D_m/D_p = 3.3$ manholes. In square manholes with $L_m/D_p = 7.8$, where L_m is the length of one side of the manhole, Jimoh et al. (2014) reported $S' = 0.24L_m$. Benched manholes tend to exhibit short-circuiting regardless of geometry and surcharge depth (Sonnenwald, 2014).

Residence time distributions (RTDs) describe mixing in manholes independent of the upstream concentration profile (Stovin et al., 2010; Guymer and Stovin, 2011; Stovin et al., 2013). The RTD quantifies the hydrodynamics and hence mixing in a system resulting from an instantaneous input (Danckwerts, 1953; Levenspiel, 1972). Convolving the RTD with an upstream concentration profile produces a downstream concentration profile. The inverse process, deconvolution, can be used to obtain the RTD from experimental upstream and downstream concentration profiles (Sonnenwald et al., 2015). Deconvolved RTDs can nearperfectly describe the mixing within manholes (Guymer and Stovin, 2011). The cumulative residence time distribution (CRTD), F, is the cumulative sum of the RTD.

The RTD and CRTD are commonly analyzed in dimensionless time, tQ/V, where V is the volume of water between the upstream and downstream measurement locations x_1 and x_2, and Q is the discharge. The nominal retention time $t_n = V/Q$ occurs at $tQ/V = 1$ and represents the amount of time needed for all particles of water to travel between x_1 and x_2 at a uniform velocity, i.e., plug flow. Dimensionless time has been used to show that mixing in manholes is independent of manhole diameter, flow rate, and surcharge depth when either below- or above-threshold (Stovin et al., 2010; Guymer and Stovin, 2011; Stovin et al., 2013).

The hydrodynamics between the upstream and downstream measurement locations can be interpreted by visual inspection of the CRTD. This is illustrated in Fig. 2. Complete instantaneously well-mixed flow (e.g., a continuously stirred tank) results in an exponential CRTD ($F = 1 - \exp(tQ/V)$). A steep rise in the CRTD, where much of the flow has the same travel time, indicates a preferential flow path. If a steep rise occurs at $tQ/V < 1$, this indicates short-circuiting, with the height of the rise indicative of the amount of short-circuiting. Short-circuiting often occurs when there is a dead zone or recirculation cell. A long gentle CRTD tail indicates dead-zone trapping. When the exchange between the main flow path and dead zone is high, the tail of the CRTD is shorter/steeper.

Guymer and Stovin (2011) utilized deconvolution to obtain CRTDs directly from experimental manhole solute trace data. The study synthesized these CRTDs to a single below- and above-threshold CRTD pair that could be used to predict mixing across circular unbenched straight-through $4.4 \leq D_m/D_p \leq 9.1$ manholes, validated for $D_m/D_p = 9.1$. This empirical model has limited transferability as it requires knowledge of the threshold depth, which changes with manhole configuration.

Following Guymer et al. (2005), Stovin et al. (2013) hypothesized that the change in flow regime in manholes with respect to D_m/D_p and surcharge depth, i.e., the occurrence of the threshold, could be explained using jet theory. A submerged circular jet entering a semi-infinite volume takes on the shape of an expanding cone, with water moving less rapidly towards the edges of the cone (Albertson et al., 1950; Rajaratnam, 1976). In the center is a jet core, which is a cone decreasing in diameter but with an approximately uniform velocity equal to the inlet velocity. The expanding cone that makes up the jet, excluding the jet core, is referred to as the jet diffusion zone. It is caused by the momentum that enters with the jet gradually transferring into the surrounding water, expanding at a rate of approximately 1 in m where $m = 5$ (Albertson et al., 1950). The distance the jet core penetrates a volume of water is controlled by the diameter of the jet's inlet, such that $L_j = D_p/(2\alpha_2)$ where L_j is the length of the jet core and α_2 is the rate of jet core dissipation. The values of α_2 reported in the literature vary, with values reported by Gauntner et al. (1970) and Rajaratnam (1976) ranging between $1/15.4 < \alpha_2 < 1/9.4$ with most values around 1/12. The region where the jet core remains is referred to as the zone of establishment, and the region after the jet core is fully dissipated is referred to as the zone of established flow.

Albertson et al. (1950) reported $\alpha_2 = 1/12.4$, giving $L_j = 6.2D_p$. Stovin et al. (2013) therefore concluded, in agreement with their modelling results, that in smaller diameter manholes, $D_m/D_p < 6.2$ or $D_m < L_j$, the jet core would always reach the outlet and short-circuit. At larger diameters, Stovin et al. (2013) proposed that below-threshold the expanding edge of the jet diffusion zone would reach the surface and disturb the manhole volume, leading to the observed complete mixing (Fig. 1a). At higher surcharges above-threshold, they proposed that the overlying surcharge and 3D effects would tend to dampen the flow field and the jet would continue to the outlet uninterrupted and thus short-circuit (Fig. 1b). With the jet diffusion zone expanding at a rate of 1 in 5, the manhole surface would be reached at $0.2D_m$, which Stovin et al. (2013) found to agree reasonably well with $S' = 0.258D_m$.

Using jet theory, Mark and Ilesanmi-Jimoh (2017) divided the volume of a manhole into three zones: jet core, jet diffusion, and outer mixing (the remaining manhole volume). They applied the submerged jet theory associated with each zone to create a three-zone compartmental mixing model (Chapra, 1997) where mixing between the zones is driven by mass flux. Velocity at the plane of the outlet of the jet core and jet diffusion zones was calculated based on Albertson et al. (1950) and integrated to calculate flow. By multiplying the integrated flow at the outlet plane with the concentration within the zone, the mass flux out of both zones was calculated. In the Mark and Ilesanmi-Jimoh (2017) model, flow (Q) from the manhole inlet (V_0) enters the manhole in the jet core zone (V_1) and is either transported into the jet diffusion zone (V_3) as $Q_{1,3}$ or continues to the outlet (V_2) as $Q_{1,2}$. Flow from V_1 to V_2 ($Q_{1,2}$) is determined by integrating the jet core velocity at the outlet plane. The remaining outflow comes from the jet diffusion zone ($Q_{3,2}$). The jet diffusion zone flow that does not exit via the outlet is instead exchanged with the outer mixing zone (V_4) as $Q_{3,4}$. Mass-balance in the model is achieved using the return flow from the outer mixing zone to jet diffusion zone $Q_{4,3}$. This is illustrated in Fig. 3a-b. The Mark and Ilesanmi-Jimoh (2017) model is analogous to an ADZ model with multiple zones. While the model is an analytical framework for predicting mixing and was designed for circular unstepped and stepped straight-through manholes, the model only applies to manholes with $D_m < L_j$. Mark and Ilesanmi-Jimoh (2017) compared results against a small dataset of just five solute traces, giving limited confidence in its general applicability. To date, a generalized model for predicting mixing across the wide range of surcharged manhole configurations encountered in practice has not been presented.

The Guymer et al. (2020) dataset is a large database of solute traces in manholes, consisting of over 4,000 traces in circular manholes and their corresponding CRTDs for over

1,000 experimental conditions, varying both hydraulic conditions (flow rate and surcharge depth) and manhole geometry (diameter, step height, and outlet angle). Although the dataset is incomplete for benched manholes, the unbenched manholes provide a baseline case for model development. Additionally, while design guidance suggests manholes with ratios $D_m/D_p \approx 3$ to be most common in networks (WRC, 2012), the results of Stovin et al. (2013) suggest manholes of this size perform similarly to the $D_m/D_p = 4.4$ manholes covered within the dataset. Larger ratios may also be more common upstream in networks where pipe diameters are smaller and a minimum manhole diameter is fixed. Therefore, using the unbenched manhole data from the Guymer et al. (2020) dataset, this study aims:

- to further develop the compartmental modelling approach of Mark and Ilesanmi-Jimoh (2017) to describe mixing across manholes for a range of D_m/D_p ratios, stepped manholes, and angled manholes;
- to confirm compartmental modelled CRTDs are consistent with experimental CRTDs and represent the relevant hydrodynamics across the extensive Guymer et al. (2020) dataset, identifying any limitations; and
- to demonstrate the compartmental model offers an improved representation of mixing in manholes compared to the instantaneously well-mixed assumption.

EXPERIMENTAL WORK

The Guymer et al. (2020) dataset, as previously mentioned, contains experimental manhole solute traces (upstream and downstream temporal concentration profiles) collected by O'Brien (2000), Dennis (2000), Saiyudthong (2004), Guymer et al. (2005), and Lau (2008) from a variety of circular manhole configurations. The data covers a range of manhole diameters, inlet pipe diameters, flow rates, surcharge depths, outlet step heights, and outlet angles. The range of manhole configurations utilized in this study is outlined in Table 1. Between two and eight repeat traces were conducted with Rhodamine dye and recorded with

Series 10 Turner Design fluorometers located on inlet and outlet pipes a short distance upstream and downstream of the manhole. The surcharge level was controlled with a downstream weir and measured with an Armfield Limited H45 mechanical water surface level follower. Both the fluorometers and water level follower were logged by PC using either a Cambridge Electronic Design CED 1401 or Measurement Computing Corporation CIO-DAS802. Flow rate was either measured using a point depth gauge over a calibrated 30° V-notch weir built to BS 3680-4A:1981 (BSI, 1981) or a venturi meter based on BS EN ISO 5167-1:2003 (BSI, 2003). Smooth pipes were used with a relative roughness of approximately 2×10^{-5} and a friction factor of 0.020.

The dataset also contains CRTDs deconvolved from the trace data according to Sonnenwald et al. (2015), which is based on maximum entropy deconvolution (Skilling and Bryan, 1984). To deconvolve, a non-linear optimizer is used to maximize the entropy of a sub-sampled RTD while constrained to goodness-of-fit between the downstream concentration profile predicted using the reconstructed RTD and the measured downstream profile. This may be expressed in a Lagrangian function, which was solved using the MATLAB *fmincon* function (The MathWorks Inc., 2020). The RTD is reconstructed from the sub-sampled RTD using a smoothed interpolation approach. The deconvolution method was modified by Guymer et al. (2020) to permit dynamic sample point number selection and to utilize a slope-based sampling point scheme that allows for RTDs shorter than the recorded data.

The trace data have been pre-processed to apply the reported calibrations, filter noise, subtract background concentration, and trim the traces. A low-pass Butterworth filter was applied using the MATLAB *butter* function (The MathWorks Inc., 2020) with a 1 Hz cut-off frequency to remove high-frequency sensor noise. Background was taken as the mean of the first and last 10 seconds of data. A copy of the trace was smoothed with a moving average and used to determine the start time of the trace as 1% of the smoothed peak upstream profile and the end of the trace as 1% of the peak of the smoothed downstream profile.

Manhole data with mass-balance less than 0.6 or greater than 1.1 have not been processed, except for 60° outlet angle data where mass-balance was assumed due to missing sensor calibrations (83 traces). Configurations with dissimilar CRTDs between repeat traces have also not been processed (31 configurations). These typically occurred near the threshold and indicate the flow field was changing between repeats. The 800 mm manhole configurations reported by O'Brien (2000) have also not been processed, as the traces were of insufficient duration to record the complete downstream trace (25 configurations). CRTDs were scaled to have a final value of 1 when the final value exceeded 1. Finally, the CRTDs for each repeat trace were averaged to produce a single mean CRTD for each configuration.

MODEL DEVELOPMENT

Several changes have been made and new process descriptions added to the compartmental model of Mark and Ilesanmi-Jimoh (2017). The new developments are intended firstly to improve: estimates of zone volumes; estimates of exchange between zones; and the description of jet deflection in stepped manholes. Secondly, the model has been extended to apply to: very high surcharge levels; large diameter manholes ($D_m \geq L_j$); and angled manholes. Fig. 3 details the compartmental model zones, their notation, relationships between them, and geometry for an unbenched circular manhole.

Mark and Ilesanmi-Jimoh (2017) calculated the volume of the jet core (V_1) and jet diffusion zone (V_3) as simple cones, and while the volumes extending beyond the inlet and outlet (V_{1b} and V_{3b}) were accounted for, they did not account for the jet diffusion zone extending below the bottom of the manhole (V_{3c}) or above the water surface (V_{3d}). These volumes have now been accounted for. By considering the bottom of the manhole and water surface, the flow from the jet diffusion zone to the outer mixing zone ($Q_{3,4}$) has also been reduced compared to the Mark and Ilesanmi-Jimoh (2017) model.

In stepped manholes, vertical jet deflection towards the outlet was observed in some LIF images presented by Dennis (2000). Mark and Ilesanmi-Jimoh (2017) proposed to calculate the jet angle as the resultant of mean downwards velocity and mean horizontal jet velocity, giving jet deflection on the order of 10°. However, empirical relationships for jet crossflow (where a jet enters a perpendicular flow) given by Rajaratnam (1976) suggest jet deflection of less than 1°. Agelin-Chaab and Tachie (2011) described the behavior of round offset jets, which are analogous to the inlet jet in a stepped manhole, in a semi-infinite volume. They found the edge of the jet diffusion zone to hit the bed at a relatively short distance from the inlet, spreading to the bed more rapidly than into an infinite volume. Although the jet core similarly deflects towards the bed, at small jet offsets ($B/D_p \leq 1$) the jet core does not deflect significantly until 10 jet diameters ($10D_p$) from the inlet. As the jet inlet moves further from the bed (increasing jet offset or manhole step height) the distance before jet deflection increases. As with jets into a semi-infinite volume, this behavior is independent of flow rate, scaling with inlet diameter and jet offset. Both crossflow jet and offset jet behavior suggests that jet deflection due to a step would be minimal within the diameter of a manhole. To be consistent in the use of jet theory and to simplify model geometry, we, therefore, have not included jet deflection in either stepped or angled manholes.

In a stepped manhole, the outlet invert is at a lower elevation B than the inlet invert. Without jet deflection then, the jet core and outlet are not aligned and as B increases eventually the jet diffusion zone will not entirely overlap the outlet (Fig. 3f). In this case, as outlined by Mark and Ilesanmi-Jimoh (2017), the position of the outlet relative to the jet core and jet diffusion zone is used to determine the proportion of flow each zone contributes to the outlet. Any flow not from the jet core or jet diffusion zone comes from the outer mixing zone ($Q_{4,2}$).

Fig. 4a shows a recorded downstream concentration profile compared to a downstream concentration prediction made using the Mark and Ilesanmi-Jimoh (2017) model and a prediction made using the new estimates of zone volume and exchange. Fig. 4b shows the effect of assuming no vertical jet deflection. Goodness-of-fit between the experimental and modelled downstream concentration profiles has been evaluated using the R_t^2 correlation coefficient (Young et al., 1980). In both examples, the changes made for the new compartmental model increase the quality of the downstream prediction.

The new compartmental model incorporates a new 'high-surcharge storage' zone (V_5) when surcharge depth exceeds manhole diameter. LIF images of dye in high-surcharge manholes, presented by Dennis (2000), suggest that in such conditions little dye reaches the upper level of the surcharge. Habib et al. (2005) investigated flow in dead-end pipe legs and showed that counter-rotating recirculation cells could form in similar hydraulic conditions. Assuming counter-rotation, recirculation in the outer mixing zone would be mirrored in the high-surcharge storage volume. Hence, the upwards and downwards exchange between the outer mixing zone and the high-surcharge zone ($Q_{4,5}$ and $Q_{5,4}$) have been assumed to be equal to the downwards exchange between the outer mixing zone to the jet diffusion zone ($Q_{4,3}$).

In a large diameter manhole ($D_m > L_j$), the jet core no longer reaches the outlet (shown in Fig. 3e) and extending the reasoning applied to a stepped manhole, the jet core zone contributes entirely to the jet diffusion zone. In turn, the latter contributes entirely to the outlet. To calculate contributions to the outlet and flow between zones in angled manholes, with an outlet turned through θ degrees (shown in Fig. 3g), again a similar approach to a stepped manhole was used. If the outlet is 90° to the inlet, the outlet is only in contact with the outer mixing zone, and flow must pass through the jet core, jet diffusion zone, and outer mixing zone to reach the outlet. In general, the location of the outlet should be compared with the locations of the jet core and jet diffusion zones to determine proportional flow contributions to the outlet.

For comparison of model results to the experimental data, it is necessary to account for the fluorometers being located on the inlet and outlet pipes just before and after the manhole, rather than directly at the inlet and outlet. To account for the varying length of pipe between experimental configurations, we assume pipe dispersion is negligible compared to mixing caused by the manhole, and thus it only necessary to account for the advection within the pipe. This may be achieved with a time delay term, which Rutherford (1994) defined as the difference in the first arrival time of a tracer between an upstream and downstream measurement location. Time delay has been estimated as the length of the pipe sections divided by peak pipe velocity U_{max}, i.e., $(x_2 - x_1 - D_m)/U_{max}$, with $U_{max} \approx 1.14U$ assuming a logarithmic turbulent pipe velocity profile. This can be converted to dimensionless time, similar to the CRTD, using tQ/V, where V is the total volume of water between x_1 and x_2. The mean experimental dimensionless time delay for the experimental data was 0.15, taken as t_1 from the CRTD, the time at which 1% of material entering the manhole has exited. The mean estimated dimensionless time delay was 0.19. This is an overestimate of 23% compared to the experimental value but given experimental manhole CRTDs typically have a dimensionless time duration of 3 or longer, the difference in time delay is around only 1% of CRTD duration and thus an acceptable approximation.

The new compartmental model has been implemented in MATLAB (The MathWorks Inc., 2020). V_3 has been approximated as a cone that partially extends beyond the edge of the manhole, shown outside the boundaries of the manhole in Fig. 3c. The flow rates between zones relating to V_3 are affected by this simplification. The solution used to estimate the reduction in flow due to the bottom of the manhole is also an approximation. These approximations, when compared to using high-resolution numerical integration affect their respective quantities by 2-3%, depending on the exact manhole geometry. Fig. 5 shows the effect of changing V_3 and $Q_{3,4}$ by ±5%, represented by the shaded areas, on a compartmental modelled CRTD. The CRTD was calculated directly from the compartmental model as the cumulative response to a single time step upstream pulse input. Given the variation in α_2 values reported in the literature, Fig. 5 also shows the effect of changing α_2 by ±5%. Of the three, the new compartmental model is most sensitive to changes in $Q_{3,4}$. The model is insensitive to small changes in V_3 and α_2. Sonnenwald et al. (2021) provide the code used for the new compartmental model, as well as further details on calculating the zone volumes, the exchange between zones, and model solution.

RESULTS

Comparison of experimental and modelled CRTDs

Fig. 6 compares modelled CRTDs with the deconvolved experimental CRTDs for the straight-through $D_m/D_p = 4.4$, straight-through $D_m/D_p = 9.1$, stepped $B/D_p = 1.5$, and 90° angled outlet manholes (the latter two are both $D_m/D_p = 4.4$). The remaining CRTDs are shown in Figs. S1–S3 in the supplementary material. In all cases, the trend of decreasing tQ/V at the start of the CRTD with increasing surcharge is reproduced. The modelled CRTDs also become more angled with increasing surcharge, similar to the experimental CRTDs.

The agreement between the experimental and modelled CRTDs is particularly good for the straight-through $D_m/D_p = 4.4$ manholes, Figs. 6a and 6b. As manhole diameter increases to $D_m/D_p = 9.1$ (Figs. 6c and 6d), the experimental CRTDs fall into two clear groups above and below $S/D_m \approx 0.27$, corresponding to below-threshold and above-threshold flow conditions. As surcharge increases, the modelled CRTDs do indicate increased levels of short-circuiting. However, this is far less obvious than in the experimental data. In both the stepped $B/D_p = 1.5$ (Figs. 6e and 6f) and 90° angled (Figs. 6g and 6h) manholes, there is no clear separation of below- and above-threshold experimental or modelled CRTDs. In both sets of experimental data, though, there is a slight deviation around $F \approx 0.4$ that is not reproduced by the model.

Fig. 7 shows t_{10}, t_{50}, and t_{70} residence times (when 10%, 50%, and 70% of the material entering the manhole has exited) for the experimental deconvolved and modelled CRTDs with respect to surcharge ratio S/D_m. For the straight-through D_m/D_p > 4.4 manholes, the difference between the experimental and modelled values for t_{10} (Fig. 7a) is generally small and consistent with the differences in estimated time delay. However, the experimental values of t_{50} (Fig. 7d) show a discontinuity at $S/D_m \approx 0.27$, consistent with the results of Stovin et al. (2013). The model does not predict the sharp drop in t_{50} at the threshold surcharge depth, which is consistent with the lack of differentiation between below- and above-threshold CRTDs in Fig. 6d. At t_{70} (Fig. 7g) the scatter in the experimental residence times for straight-through $D_m/D_p = 4.4$ manholes corresponds to the plateau shown in the experimental CRTDs in Fig. 6a at $F \approx 0.7$.

In the stepped manholes, t_{10} (Fig. 7b) is estimated well, except for $B/D_p = 2.0$. t_{50} and t_{70} (Figs. 7e and 7f) are also overestimated for the largest step height configurations. Modelled t_{50} and t_{70} both decrease with $S/D_m > 1$, reflecting the influence of the high-surcharge storage zone.

Residence times are predicted reasonably well for angled manholes, except for t_{70} (Fig. 7i) in the 30° angled manhole. t_{10} (Fig. 7c) is overestimated in the angled manholes at $S/D_m \lesssim 0.4$, which could be a result of the flow path cutting the corner between the inlet and the outlet. The experimental t_{50} (Fig. 7f) values for the 30° angled and t_{10} for the 60° and 90° angled manholes show a systematic decrease above $S/D_m \approx 0.7$ that is consistent with the threshold between well-mixed and short-circuiting flow conditions reported by Sonnenwald (2014).

Comparison with the instantaneously well-mixed model

Fig. 8 compares CRTDs generated using the new compartmental model with both the experimental CRTDs and the instantaneously well-mixed model CRTDs for selected manhole configurations (see Table S1 in the supplementary material). Mean pipe travel time has been added to the well-mixed model CRTDs to account for the experimental fluorometer placement on pipe lengths upstream and downstream of the manhole. Figs. 8a and 8b show results for straight-through manholes, Figs. 8c and 8d stepped manholes, and Figs. 8e and 8f angled manholes. The left-hand plots show below-threshold CRTDs, while the right-hand plots show above-threshold CRTDs. Note, for straight and stepped manholes the threshold depth of $S' = 0.258D_m$ has been used, and for angled manholes $S' = 0.7D_m$.

Overall, it is clear that the new compartmental model provides significantly better estimates of the experimental CRTDs than the well-mixed exponential model, which does not estimate any of the observed short-circuiting effects.

As the manhole geometry deviates from a small diameter straight-through manhole, the experimental CRTDs tend to show more complete mixing at low surcharges. This is demonstrated in Fig. 8a, where the fit of the well-mixed model improves as the D_m/D_p ratio increases for below-threshold cases. However, as highlighted in the discussion of Fig. 6, the compartmental model is not fully able to capture the short-circuiting effects that were experimentally observed in larger diameter above-threshold conditions (Fig. 8b).

In below-threshold geometries when the manhole is similar to a straight-through narrow manhole, e.g., the stepped $B/D_p = 0.5$ manhole, short-circuiting occurs, and the new compartmental model reflects this (Fig. 8c). The transition to complete mixing in stepped manholes is likely driven by the jet deflecting slightly for small changes in outlet alignment (Dennis, 2000; Beg et al., 2019) until it no longer deflects and instead impacts the far wall of the manhole, disrupting the flow field (Sonnenwald, 2014).

Whilst there appear to be some inconsistencies in the compartmental model's ability to predict the tail of the CRTD, i.e., the amount of dead-zone exchange, compared to the experimental CRTDs, it is believed that this reflects experimental limitations, either in the premature termination of experimental traces or due to insufficient sensitivity in the measurement systems.

Concentration profiles

The new compartmental model and the well-mixed model were applied to make downstream predictions for 3,941 recorded solute traces. Overall, the compartmental model underpredicted peak concentrations by 10% on average, compared with 60% by the well-mixed model. Goodness-of-fit between the measured and modelled downstream concentration profiles was evaluated using R_t^2. The compartmental model created good engineering predictions for the available data with a mean R_t^2 of 0.881, a standard deviation of 0.119, and a median of 0.917, compared with 0.667, 0.180 and 0.697 respectively for the complete mixing assumption. Across all traces, the compartmental model R_t^2 tended to decrease with increasing manhole diameter, step, and angle, i.e., as manhole geometry deviated further from an ideal straight-through small diameter manhole. This is consistent with the trends observed in the modelled CRTDs.

Fig. 9 shows a selection of recorded downstream traces compared with both the new compartmental and well-mixed model predictions (the upstream traces are not shown for clarity). These traces match the manhole configurations of the CRTDs shown in Fig. 8. Corresponding R_t^2 values are given in Table 2. The tails of some experimental traces, e.g., Fig. 9d and 9e, show oscillations that indicate recirculation within the manhole (Stovin et al., 2010). As expected, the compartmental model does not reproduce this behavior, but the otherwise good agreement between the experimental and modelled tails offers some evidence that the compartmental model predicts dead-zone exchange well.

Below-threshold, the new compartmental modelled concentration profiles are generally good fits, whilst peak concentrations are underpredicted in some above-threshold cases (e.g., Fig. 9g). In contrast, the well-mixed model provides significantly poorer predictions, underpredicting peak concentrations in all cases. The example traces shown in Fig. 9 and corresponding R_t^2 values in Table 2 confirm that the new compartmental model offers a definite improvement over the well-mixed model.

DISCUSSION

Model limitations

The compartmental model has been shown to predict mixing for a wide range of circular unbenched $4.4 \le D_m/D_p \le 9.1$, $0 \le B/D_p \le 2.0$, and $0° \le \theta \le 90°$ manhole configurations. The main limitation of the compartmental model is the underestimation of short-circuiting in high-surcharge wide, stepped, and angled manholes, which leads to underestimated peak concentrations. The compartmental model does not account for the more complex hydrodynamics occurring in these instances, and the underestimation of short-circuiting is to be expected given the model's relatively large zones used and the assumption of instantaneous mixing in each zone.

In the case of above-threshold large diameter manholes, the limitation noted above could potentially be addressed by increasing the length of the jet core assumed in the model, although further work would be required to justify such a modification. Within stepped and angled manholes, further investigation of jet behavior may also offer additional insight.

Benched manholes and manholes with multiple inlets and outlets or differing inlet and outlet diameter have not been considered here, however, the concepts of the new compartmental mixing model could be applied to these conditions by considering the manhole geometry in relation to the inlet jet.

Practical application

Although short-circuiting is underestimated by the new compartmental model, the well-mixed model currently used in commercial sewer network modelling packages predicts no short-circuiting at all and thus will tend to underestimate peak concentrations associated with the transport of transient pulses of pollutants. The new compartmental model, therefore, represents a significant improvement, predicting higher, more realistic concentrations. Notably, the new compartmental model will predict short-circuiting in $D_m/D_p \leq 4.4$ manholes, which are common in practice.

A further application of the modelling approach described here lies in its potential use for estimating energy losses due to manholes. Pedersen and Mark (1990) used a related jet-theory derived approach to estimate head losses in manholes, and their approach could be combined with the compartmental model to investigate the link between head losses and mixing previously highlighted by Stovin et al. (2013).

CONCLUSIONS

Previous investigations into mixing in surcharged manholes have failed to develop a robust model for predicting the effects of different geometry, surcharge, and discharge on mixing conditions. Current commercial modelling approaches assume instantaneous complete mixing, which cannot predict short-circuiting and underestimates peak pollutant concentrations. In this paper, a compartmental model for predicting mixing within manholes, based on submerged jet theory, has been further developed to account for a range of inlet to manhole diameter ratios (D_m/D_p), outlet steps, and outlet angles, with varying surcharge and discharge. The model performance was evaluated with over 850 manhole configurations.

The new compartmental model was shown to predict cumulative residence time distributions (CRTDs) consistent with experimental CRTDs. The model reproduced the expected short-circuiting flow conditions below- and above-threshold in straight-through small D_m/D_p manholes. As D_m/D_p, step, or outlet angle increased, below-threshold the model predicted the observed complete mixing. Above-threshold, the model showed less short-circuiting than observed. In general, as manhole geometry deviated from a straight-through small D_m/D_p manhole, or from below-threshold conditions, the agreement between experimental and modelled CRTDs decreased.

The new compartmental model successfully predicted downstream concentration profiles both below- and above-threshold. Peak concentrations were underpredicted when the compartmental model underestimated short-circuiting. The mean goodness-of-fit, using R_t^2, was 0.881 for the new compartmental model, showing significant improvement compared to 0.661 for the well-mixed model. Compared to the well-mixed model which estimates the most mixing possible, the new compartmental model will estimate more realistic, higher concentrations, for overflow impact assessments.

The new compartmental model is completely analytical and has been validated for a range of geometries. It requires no assumptions regarding mixing conditions or threshold depth, is insensitive to small changes in geometry, and as such is suitable for practical applications. For manholes outside the range investigated in this study, the jet theory used to develop the model remains relevant, as well as for other structures where an inlet jet dominates the flow field. The new compartmental model provides a robust framework to predict mixing in manholes.

DATA AVAILABILITY STATEMENT

Data and code used during this study are available in a repository online in accordance with funder data retention policies from Guymer, I., Stovin, V., O'Brien, R., Dennis, P., Saiyudthong, C., Lau, S.-T. D., and Sonnenwald, F. (2020) https://doi.org/10.15131/shef.data.13373039 and Sonnenwald, F., Mark, O., Stovin, V., and Guymer, I. (2021) https://doi.org/10.15131/shef.data.14160884.

ACKNOWLEDGEMENTS

This work was supported by the EPSRC (Grant no EP/P012027/1).

NOTATION LIST

The following symbols are used in this paper:

B = manhole outlet step size;

C = concentration;

$C_{\max}$ = peak upstream concentration;

D_m = manhole diameter;

D_p = inlet/outlet pipe diameter;

F = the cumulative residence time distribution;

L_j = the length of the jet core;

m = rate of jet diffusion zone expansion;

Q = manhole inflow or outflow rate, discharge;

$Q_{1,2}$ = flow rate from jet core to outlet;

$Q_{1,3}$ = flow rate from jet core to jet diffusion zone;

$Q_{3,2}$ = flow rate from jet diffusion zone to outlet;

$Q_{3,4}$ = flow rate from jet diffusion zone to outer mixing zone;

$Q_{4,2}$ = flow rate from outer mixing zone to outlet;

$Q_{4,3}$ = flow rate from outer mixing zone to jet diffusion zone;

$Q_{4,5} = Q_{5,4}$ =flow rate from outer mixing zone to high-surcharge storage zone and back;

R_t^2 = Young's correlation coefficient;

S = surcharge depth;

S' = threshold depth;

t = time;

t_1, t_{10}, t_{50}, t_{70} = time at which $F = 0.01$, $F = 0.1$, $F = 0.5$, $F = 0.7$;

t_{50} = median residence time;

tQ/V = dimensionless time;

U = mean pipe velocity;

V_0 = manhole inlet;

V_1 = jet core zone;

V_{1b} = volume of jet core cone extending beyond manhole outlet;

V_2 = manhole outlet;

V_3 = jet diffusion zone;

V_{3b} = volume of jet diffusion zone cone extending beyond manhole inlet;

V_{3c} = volume of jet diffusion zone extending beyond manhole floor;

V_{3d} = volume of jet diffusion zone extending beyond water surface;

V_4 = outer mixing zone;

V_5 = high-surcharge storage zone;

x_1 = upstream measurement location;

x_2 = downstream measurement location;

α_2 = the rate of jet core dissipation; and

θ = manhole outlet angle.

SUPPLEMENTARY MATERIALS

Table S1 and Figs. S1–S3 are available online in the ASCE Library (ascelibrary.org).

REFERENCES

Albertson, M. L., Dai, Y. B., Jensen, R. A., and Rouse, H. (1950). "Diffusion of submerged jets." *Transactions of the American Society of Civil Engineers*, 115(1), 639-664.

Agelin-Chaab, M. and Tachie, M. (2011). "Characteristics of turbulent three-dimensional offset jets." *Journal of Fluids Engineering*, 133(5). https://doi.org/10.1115/1.4004071

Arao, S. and Kusada, T. (1999). “Effects of pipe bending angle on energy losses at two-way circular drop manholes.” *Proc. the Eighth International Conference on Urban Storm Drainage*, International Water Association, London, 2163–2168.

BSI (British Standards Institution). 1981. *Methods of measurement of liquid flow in open channels. Part 4A: Method using thin-plate weirs*. BS 3680-4A:1981. London, UK: BSI. https://doi.org/10.3403/01558628

BSI (British Standards Institution). 2003. *Measurement of fluid flow by means of pressure differential devices inserted in circular cross-section conduits running full. Part 1: General principles and requirements*. BS EN ISO 5167-1:2003. London, UK: BSI. https://doi.org/10.3403/02774268

Beg, M. N. A., Carvalho, R. F., and Leandro, J. (2019). “Effect of manhole molds and inlet alignment on the hydraulics of circular manhole at changing surcharge.” *Urban Water Journal*, 16(1), 33-44. https://doi.org/10.1080/1573062X.2019.1611887

Butler, D., Digman, C. J., Makropoulos, C., & Davies, J. W. (2018). *Urban drainage*. CRC Press, Boca Raton, Florida.

Chapra, S. (1997). *Surface Water-Quality Modeling*. McGraw Hill Companies, Inc., New York.

Danckwerts, P. V. (1953). “Continuous flow systems: distribution of residence times.” *Chemical Engineering Science*, 2(1), 1-13. https://doi.org/10.1016/0009-2509(53)80001-1

Dennis, P. (2000). “Longitudinal dispersion due to surcharged manholes.” Ph.D. thesis, The University of Sheffield. https://etheses.whiterose.ac.uk/14802/

DHI A/S (2019). *MOUSE Pollution Transport Reference Manual*. Hørsholm, Denmark. https://manuals.mikepoweredbydhi.help/2019/MIKE_URBAN.htm

European Union Commission. (2000). “Directive 2000/60/EC of the European Parliament and of the council of 23 October 2000 establishing a framework for community action in the field of water policy.” *OJL*, 327(1), 1-73. http://data.europa.eu/eli/dir/2000/60/oj

Gauntner, J. W., Livingood, J. N. B., and Hrycak, P. (1970). “Survey of literature on flow characteristics of a single turbulent jet impinging on a flat plate.” *NASA TN D-5652*, National Aeronautics and Space Administration. https://ntrs.nasa.gov/search.jsp?R=19700009658

Guymer, I., Dennis, P., O'Brien, R., and Saiyudthong, C. (2005). “Diameter and surcharge effects on solute transport across surcharged manholes.” *Journal of Hydraulic Engineering*, 131(4), 312-321. https://doi.org/10.1061/(ASCE)0733-9429(2005)131:4(312)

Guymer, I. and O’Brien, R. (2000). “Longitudinal dispersion due to surcharged manhole.” *Journal of Hydraulic Engineering*, 126(2), 137–149. https://doi.org/10.1061/(ASCE)0733-9429(2000)126:2(137)

Guymer, I. and Stovin, V. R. (2011). “One-dimensional mixing model for surcharged manholes.” *Journal of Hydraulic Engineering*, 137(10), 1160-1172. https://doi.org/10.1061/(ASCE)HY.1943-7900.0000422

Guymer, I., Stovin, V., O’Brien, R., Dennis, P., Saiyudthong, C., Lau, S.-T. D., and Sonnenwald, F. (2020). “University of Sheffield experimental manhole traces and CRTDs. V1.” The University of Sheffield Online Research Data. https://doi.org/10.15131/shef.data.13373039

Habib, M., Badr, H., Said, S., Hussaini, I., and Al-Bagawi, J. (2005). “On the development of deadleg criterion.” *J. Fluids Eng.*, 127(1), 124-135. https://doi.org/10.1115/1.1852481

Innovyze Inc. (2019). *InfoWorks ICM 10.5 Manual*. Portland, OR. https://www.innovyze.com/en-us/products/infoworks-icm

Jimoh, M., Guymer, I., and Stovin, V. (2014). “Hydraulic threshold levels in square manholes with high length to pipe diameter ratio.” *13th International Conference on Urban Drainage*, Sarawak, Malaysia.

Lau, S.-T. D. (2008). “Scaling dispersion processes in surcharged manholes.” Ph.D. thesis, The University of Sheffield. https://etheses.whiterose.ac.uk/14935/

Levenspiel, O. (1972). *Chemical Reaction Engineering*. John Wiley & Son, Inc, New York.

Mark, O. and Ilesanmi-Jimoh, M. (2017). “An analytical model for solute mixing in surcharged manholes.” *Urban Water Journal*, 14(5), 443-451. https://doi.org/10.1080/1573062X.2016.1179335

O’Brien, R. (2000). “Dispersion due to surcharged manholes.” Ph.D. thesis, The University of Sheffield.

Obropta, C. C. and Kardos, J. S. (2007). “Review of urban stormwater quality models: Deterministic, stochastic, and hybrid approaches.” *JAWRA Journal of the American Water Resources Association*, 43(6), 1508–1523. https://doi.org/10.1111/j.1752-1688.2007.00124.x

Pedersen, F. B. and Mark, O. (1990). “Head losses in storm sewer manholes: Submerged jet theory.” *Journal of Hydraulic Engineering*, 116(11), 1317-1328. https://doi.org/10.1061/(ASCE)0733-9429(1990)116:11(1317)

Rajaratnam, N. (1976). *Turbulent jets*. Elsevier, Amsterdam.

Rossman, L. A. (2015). Storm Water Management Model User’s Manual Version 5.1. *NTIS EPA-600/R-14/413b*, US EPA Office of Research and Development, Washington, DC. https://cfpub.epa.gov/si/si_public_record_report.cfm?Lab=NRMRL&dirEntryId=310032

Rutherford, J. C. (1994). *River Mixing*. John Wiley & Son Ltd, Chichester, England.

Saiyudthong, C. (2004). “Effect of changes in pipe direction across surcharged manholes on dispersion and head loss.” Ph.D. thesis, The University of Sheffield. https://etheses.whiterose.ac.uk/14847/

Skilling, J., and Bryan, R. K. (1984). “Maximum entropy image reconstruction-general algorithm.” *Monthly Notices of the Royal Astronomical Society*, 211(1), 111-124. https://dx.doi.org/10.1093/mnras/211.1.111

Sonnenwald, F. (2014). “Identifying the fundamental residence time distribution of urban drainage structures from solute transport data using maximum entropy deconvolution.” Ph.D. thesis, The University of Sheffield.

Sonnenwald, F., Mark, O., Stovin, V., and Guymer, I. (2021). “Code for a compartmental mixing model for describing mixing in manholes. V1.” The University of Sheffield Online Research Data. https://doi.org/10.15131/shef.data.14160884

Sonnenwald, F., Stovin, V., and Guymer, I. (2015). “Deconvolving smooth residence time distributions from raw solute transport data.” *Journal of Hydrologic Engineering*, 20(11), 04015022. https://etheses.whiterose.ac.uk/5468/

Stovin, V., Bennett, P., and Guymer, I. (2013). “Absence of a hydraulic threshold in small-diameter surcharged manholes.” *Journal of Hydraulic Engineering*, 139(9), 984-994. https://doi.org/10.1061/(ASCE)HY.1943-7900.0000758

Stovin, V., Guymer, I., and Lau, S.-T. D. (2010). “Dimensionless method to characterize the mixing effects of surcharged manholes.” *Journal of Hydraulic Engineering*, 136(5), 318–327. https://doi.org/10.1061/(ASCE)HY.1943-7900.0000183

The MathWorks Inc. (2020). *MATLAB 2020a*. Natick, MA. https://www.mathworks.com/products/matlab.html

WRC. (2012). *Sewers for Adoption*. WRc Publications, Swindon, England.

Young, P., Jakeman, A. and McMurtie, R. (1980). “An instrument variable method for model order identification.” *Automatica*, 16(3), 281–294. https://doi.org/10.1016/0005-1098(80)90037-0

LIST OF TABLES

LIST OF FIGURES

5. The sensitivity of new compartmental modelled CRTDs to key model parameters $Q_{3,4}$ controlling exchange between jet diffusion zone and outer mixing zone, V_3 volume of jet diffusion zone (and hence also affecting the volume of outer mixing zone), and α_2 affecting jet core length and hence the amount of flow directly reaching outlet
6. Comparison of experimental deconvolved CRTDs (left) with new compartmental modelled CRTDs (right) for a) and b) straight-through $D_m/D_p = 4.4$, c) and d) straight-through $D_m/D_p = 9.1$, e) and f) stepped $B/D_p = 1.5$, and g) and h) 90° angled outlet manholes, CRTDs groups separated by $S/D_m \approx 0.27$ in c)
7. Comparison of experimental and new compartmental modelled dimensionless a-c) t_{10}, d-f) t_{50}, and g-i) t_{70} for a), d), g) straight-through, b), e), h) stepped, and c), f), i) angled outlet manholes (error bars on experimental data not shown, but on the order of 0.005, 0.020, and 0.050 for t_{10}, t_{50}, and t_{70} respectively)
8. Characteristic experimental, new compartmental model, and complete instantaneously well-mixed exponential model a) below- and b) above-threshold straight-through $D_m/D_p = 4.4$, $D_m/D_p = 6.8$, and $D_m/D_p = 9.1$ manhole CRTDs, c) low and d) high-surcharge stepped $B/D_p = 0.5$, $B/D_p = 1.0$, and $B/D_p = 1.5$ manhole CRTDs, e) below- and f) above-threshold 30°, 60°, and 90° angled manhole CRTDs
9. Example straight-through a) $D_m/D_p = 4.4$, d) $D_m/D_p = 6.8$, and g) $D_m/D_p = 9.1$; stepped b) $B/D_p = 0.5$, e) $B/D_p = 1.0$, and h) $B/D_p = 1.5$; and angled c) 30°, f) 60°, and i) 90° downstream below- and above-threshold/low- and high-surcharge (the latter offset by $tQ/V = 1$) downstream manhole concentration profiles with new compartmental model predictions, traces correspond to the CRTDs shown in Fig. 8, scaled by peak upstream concentration, R_t^2 values given in Table 2

Table 1. Circular manhole configurations in Guymer et al. (2020) dataset

Manhole diameter D_m (mm)	Pipe Diameter D_p (mm)	Centerline distance between fluorometers x_2 - x_1 (mm)	D_m/D_p	Flow Rate (l/s)	Surcharge Depth S (mm)	S/D_m	Outlet Angle	Step Height B (mm)	B/D_p
218	24	736	9.1	0.25–0.50	7–100	0.04–0.46	0°	0	0
388	88	2700	4.4	1.00–8.00	1–1241	0–3.20	0°, 30°, 60°, 90°	0, 44, 88, 132, 176	0, 0.5, 1.0, 1.5, 2.0
500	88	2700	5.7	0.97–7.45	7–268	0.02–0.54	0°	0	0
600	88	2700	6.8	0.87–8.72	27–308	0.04–0.51	0°	0	0
800	88	2700	9.1	0.88–8.77	27–332	0.03–0.41	0°	0	0

Table 2. Illustrative R_t^2 values comparing goodness-of-fit between recorded downstream profiles to new compartmental model and well-mixed exponential CRTD predictions, matching Fig. 9

Configuration		New compartmental model		Well-mixed exponential CRTD	
		Below-threshold	Above-threshold	Below-threshold	Above-threshold
Straight D_m/D_p	4.4	0.968	0.982	0.492	0.481
	6.8	0.932	0.863	0.847	0.324
	9.1	0.928	0.627	0.782	0.175
Stepped B/D_p	0.5	0.968	0.964	0.596	0.223
	1.0	0.956	0.896	0.729	0.460
	1.5	0.988	0.915	0.878	0.548
Angled	30°	0.909	0.707	0.556	0.254
	60°	0.732	0.510	0.687	0.530
	90°	0.944	0.792	0.863	0.833
Mean		0.927	0.925	0.806	0.714

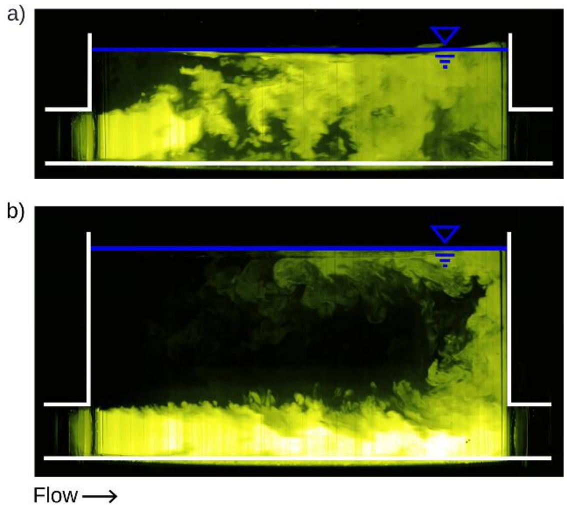

Figure 1. Vertical central plane laser-induced fluorescence imaging snapshot of dye traces through a D_m/D_p = 9.1 manhole a) below-threshold and b) above-threshold

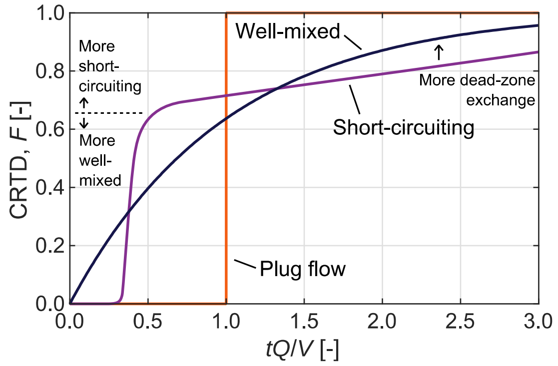

Figure 2. Example CRTDs representing different mixing processes, the short-circuiting curve indicates around 65% of the flow short-circuits ($F \approx 0.65$)

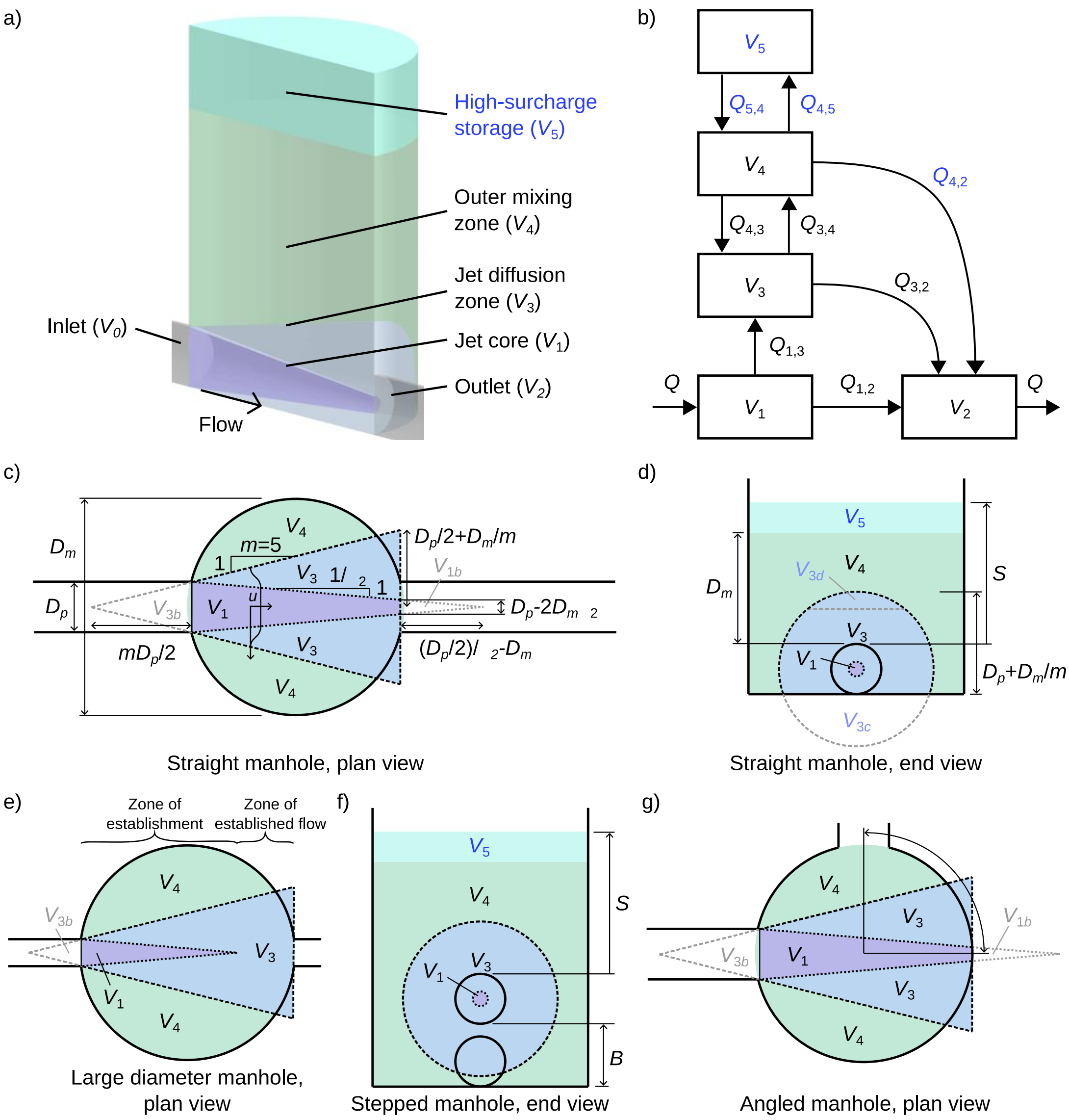

Figure 3. a) Cross-section indicating main model zones in a simple circular manhole, b) flow relationships between model zones, c) plan view (also illustrating the jet velocity profile) and d) end view of a manhole with $D_m < L_j$, e) plan view of a large manhole with $D_m > L_j$, f) end view of a stepped manhole, and g) plan view of an angled manhole, the gray areas indicate subtracted volumes, the blue text indicates new compartmental model developments, diagrams not to scale

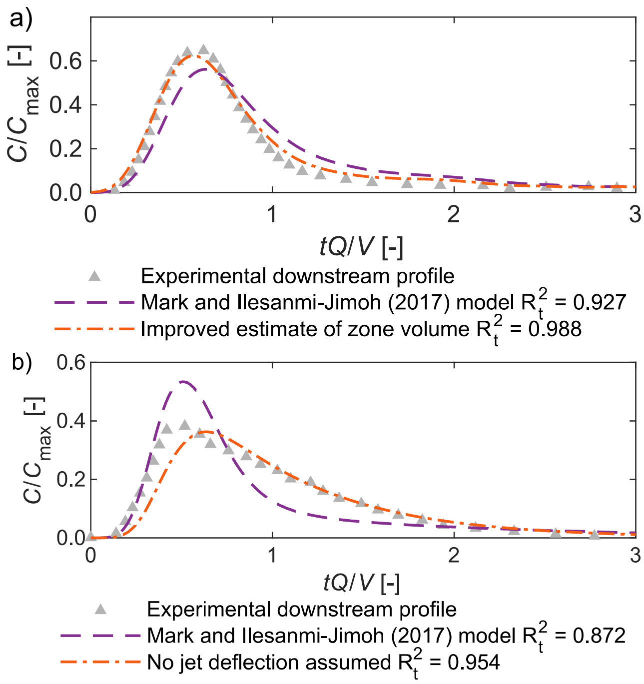

Figure 4. Illustration of a) new estimates of zone volume and exchange (in a D_m/D_p = 4.4 manhole) and b) assumption of no jet deflection (in a B/D_p = 1.5 stepped manhole) made by comparing an experimental downstream manhole concentration profile to predictions, scaled by peak upstream concentration, with R_t^2 values

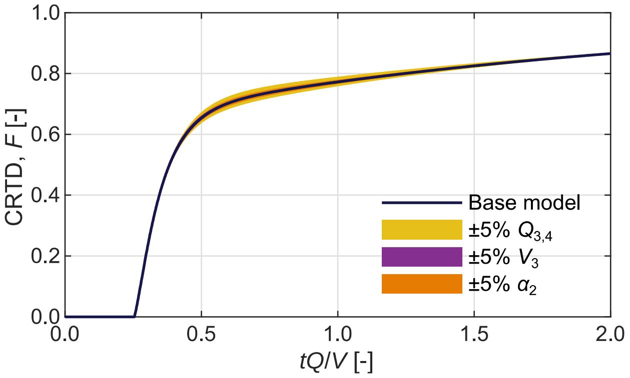

Figure 5. The sensitivity of new compartmental modelled CRTDs to key model parameters $Q_{3,4}$ controlling exchange between jet diffusion zone and outer mixing zone, V_3 volume of jet diffusion zone (and hence also affecting the volume of outer mixing zone), and α_2 affecting jet core length and hence the amount of flow directly reaching outlet

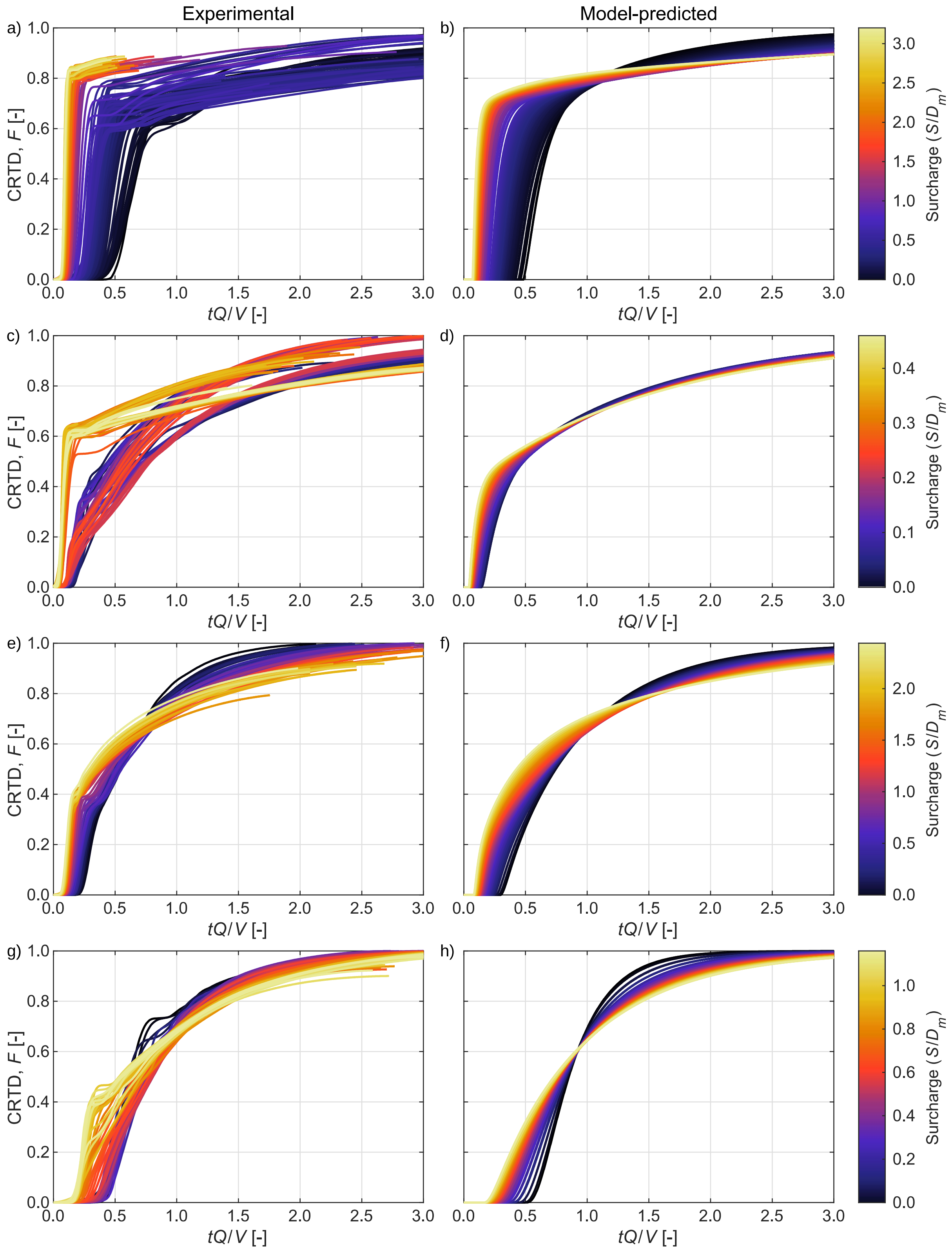

Figure 6. Comparison of experimental deconvolved CRTDs (left) with new compartmental modelled CRTDs (right) for a) and b) straight-through $D_m/D_p = 4.4$, c) and d) straight-through

$D_m/D_p = 9.1$, e) and f) stepped $B/D_p = 1.5$, and g) and h) 90° angled outlet manholes, CRTDs groups separated by $S/D_m \approx 0.27$ in c)

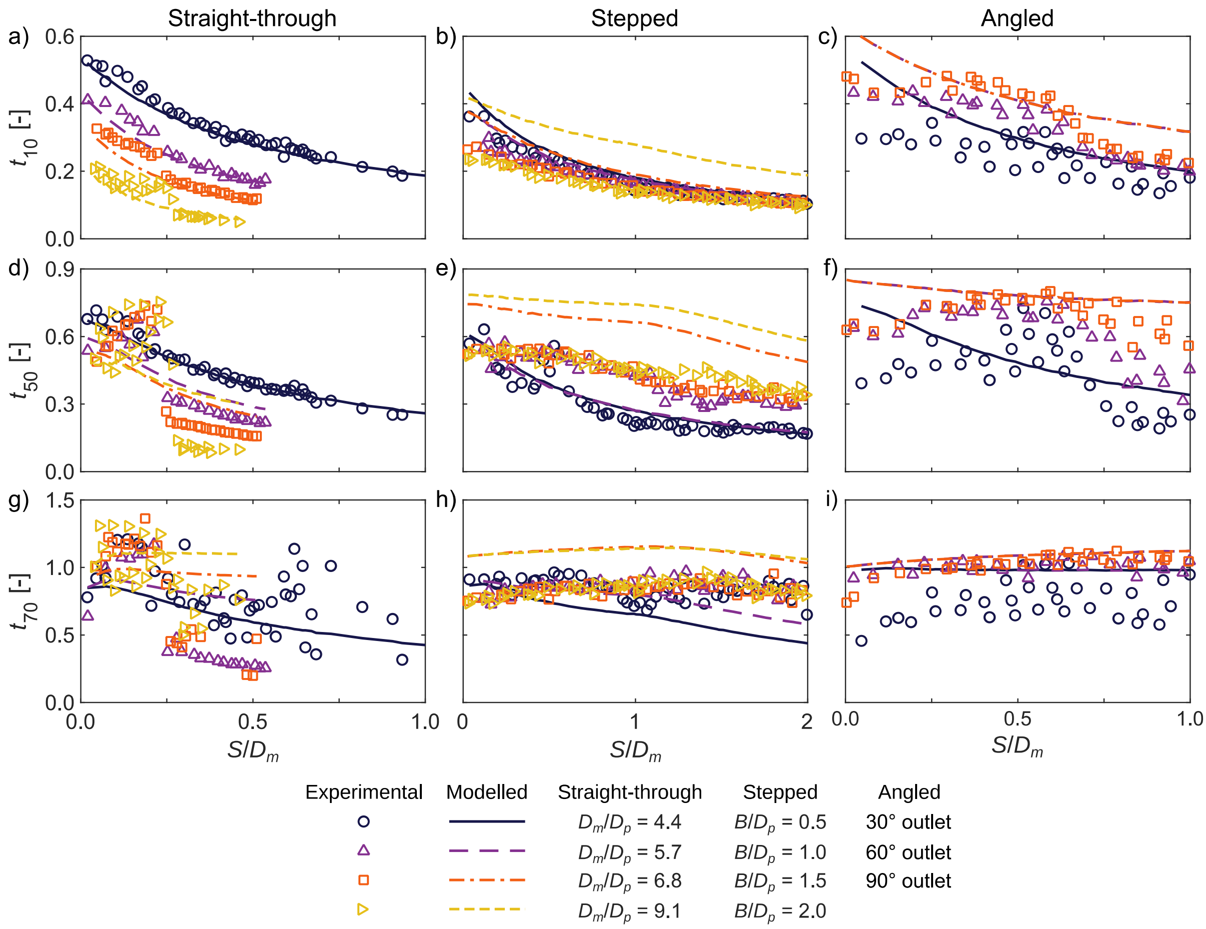

Figure 7. Comparison of experimental and new compartmental modelled dimensionless a-c) t_{10}, d-f) t_{50}, and g-i) t_{70} for a), d), g) straight-through, b), e), h) stepped, and c), f), i) angled outlet manholes (error bars on experimental data not shown, but on the order of 0.005, 0.020, and 0.050 for t_{10}, t_{50}, and t_{70} respectively)

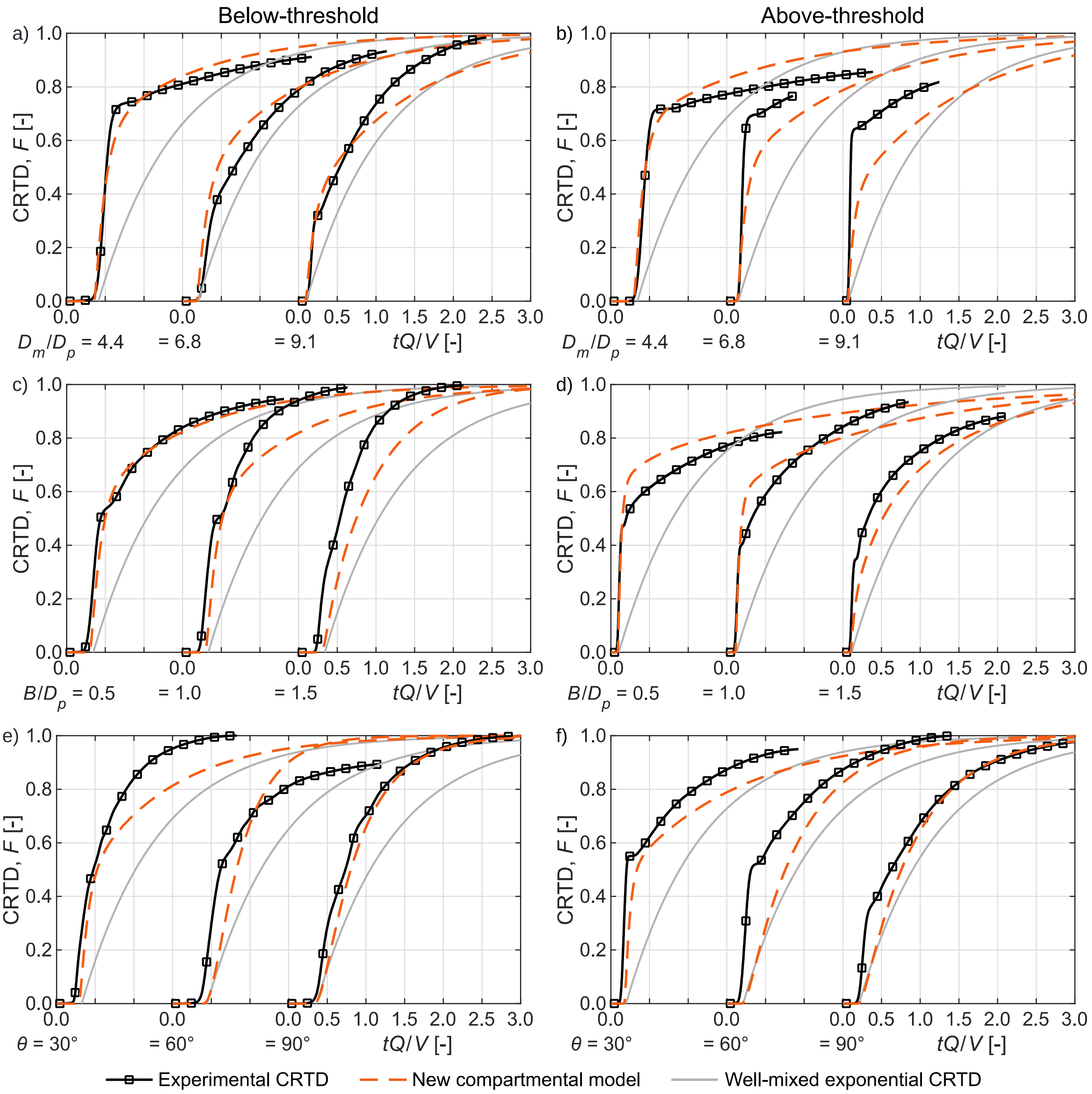

Figure 8. Characteristic experimental, new compartmental model, and complete instantaneously well-mixed exponential model a) below- and b) above-threshold straight-through $D_m/D_p = 4.4$, $D_m/D_p = 6.8$, and $D_m/D_p = 9.1$ manhole CRTDs, c) low and d) high-surcharge stepped $B/D_p = 0.5$, $B/D_p = 1.0$, and $B/D_p = 1.5$ manhole CRTDs, e) below- and f) above-threshold 30°, 60°, and 90° angled manhole CRTDs

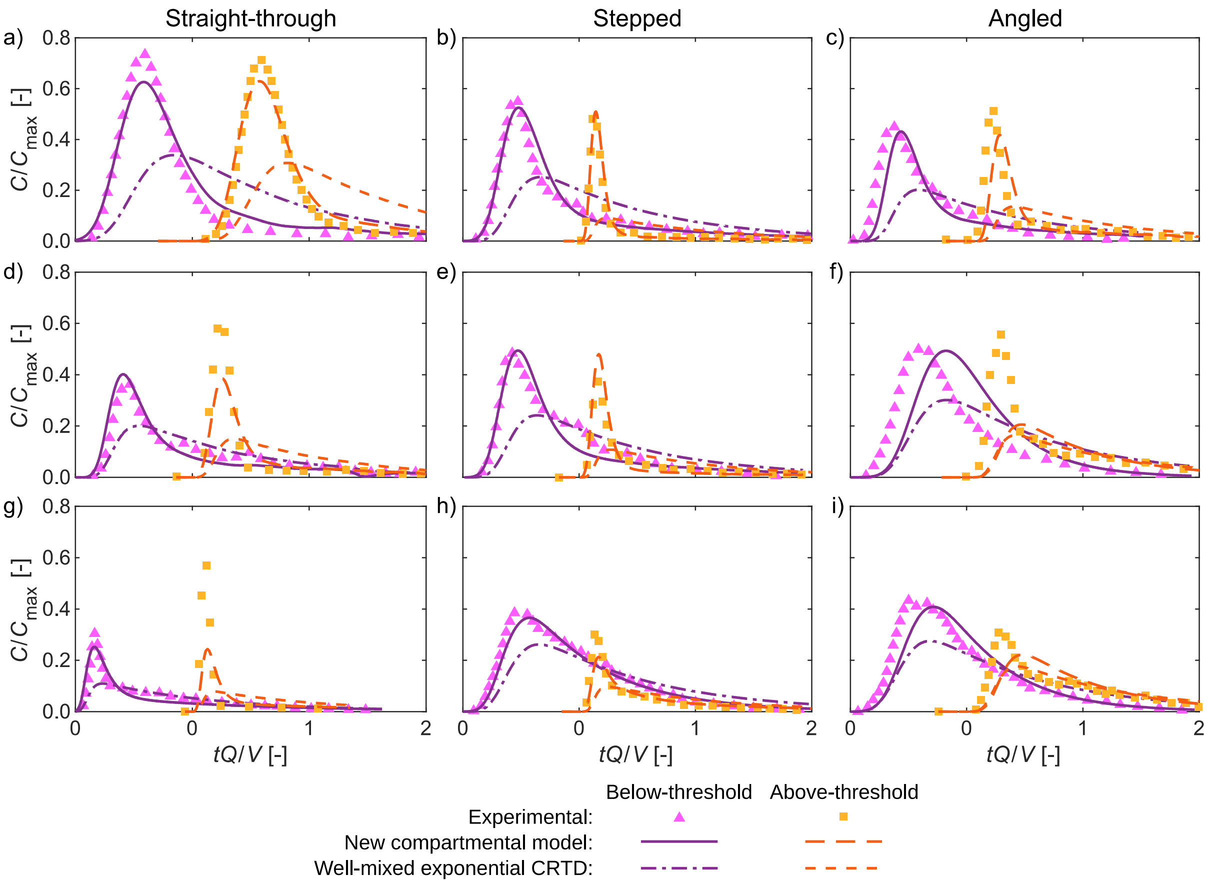

Figure 9. Example straight-through a) $D_m/D_p = 4.4$, d) $D_m/D_p = 6.8$, and g) $D_m/D_p = 9.1$; stepped b) $B/D_p = 0.5$, e) $B/D_p = 1.0$, and h) $B/D_p = 1.5$; and angled c) 30°, f) 60°, and i) 90° downstream below- and above-threshold/low- and high-surcharge (the latter offset by $tQ/V = 1$) downstream manhole concentration profiles with new compartmental model predictions, traces correspond to the CRTDs shown in Fig. 8, scaled by peak upstream concentration, R_t^2 values given in Table 2

SUPPLEMENTARY MATERIALS

Table S1. Manhole configurations details and Guymer et al. (2020) dataset Configuration ID (CID) for mean CRTDs used in Fig. 8, along with dataset File ID (FID) for the matching solute traces used in Fig. 9 (all have 88 mm diameter pipe and 2 l/s flow rate)

Fig. 8	D_m/D_p	B/D_p	Outlet Angle	S/D_m	Dataset CID	Fig. 9	Dataset FID
a	4.4	0	0°	0.21	18	a	851
	6.8	0	0°	0.15	180	d	893
	9.1	0	0°	0.15	1064	g	4484
b	4.4	0	0°	0.39	25	a	19
	6.8	0	0°	0.28	186	d	923
	9.1	0	0°	0.27	1069	g	4507
c	4.4	0.5	0°	0.24	321	b	1597
	4.4	1.0	0°	0.16	412	e	2052
	4.4	1.5	0°	0.03	496	h	2472
d	4.4	0.5	0°	2.32	329	b	1637
	4.4	1.0	0°	1.70	418	e	2082
	4.4	1.5	0°	1.84	503	h	2507
e	4.4	0	30°	0.41	880	c	3903
	4.4	0	60°	0.15	937	f	4074
	4.4	0	90°	0.31	1003	i	4272
f	4.4	0	30°	1.02	887	c	3924
	4.4	0	60°	0.92	947	f	4104
	4.4	0	90°	0.92	1011	i	4296

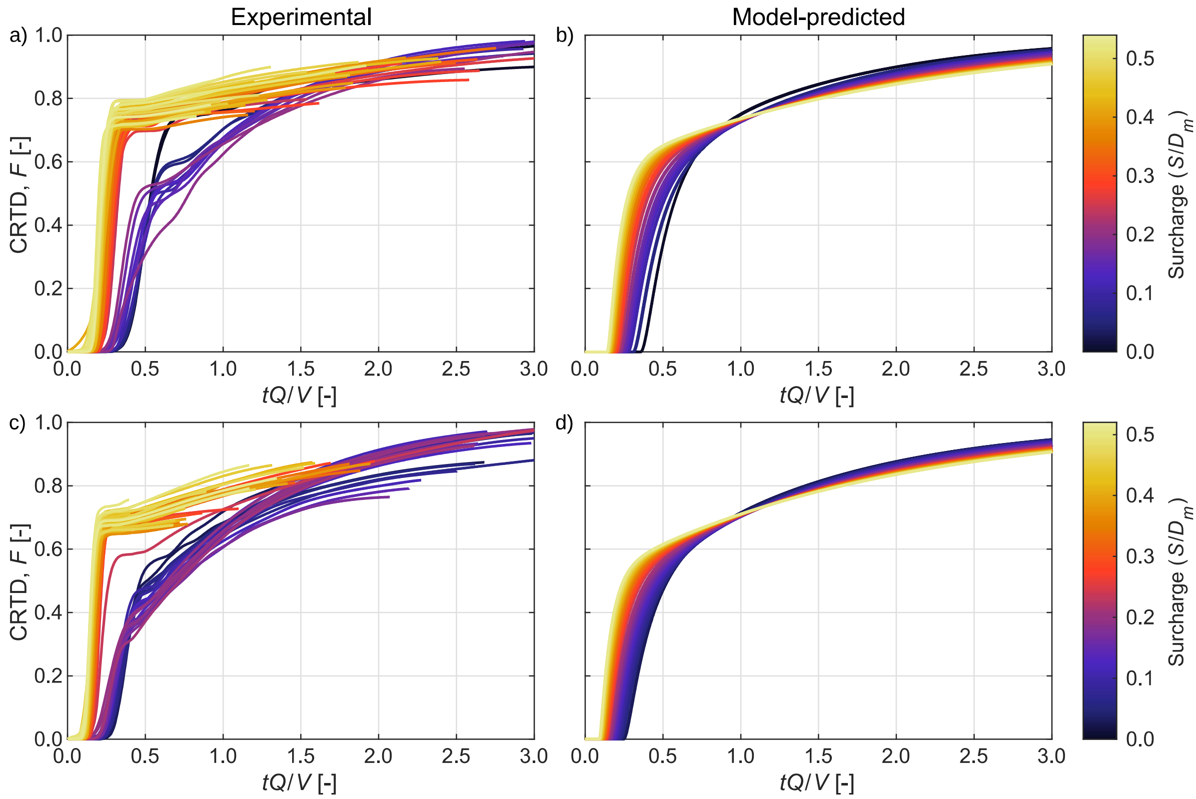

Fig. S1. Comparison of experimental deconvolved CRTDs (left) with new compartmental model predicted CRTDs (right) for straight-through a) and b) $D_m/D_p = 5.7$ and c) and d) $D_m/D_p = 6.8$ manholes, CRTDs groups separated by $S/D_m \approx 0.24$ and $S/D_m \approx 0.26$ in a) and c) respectively

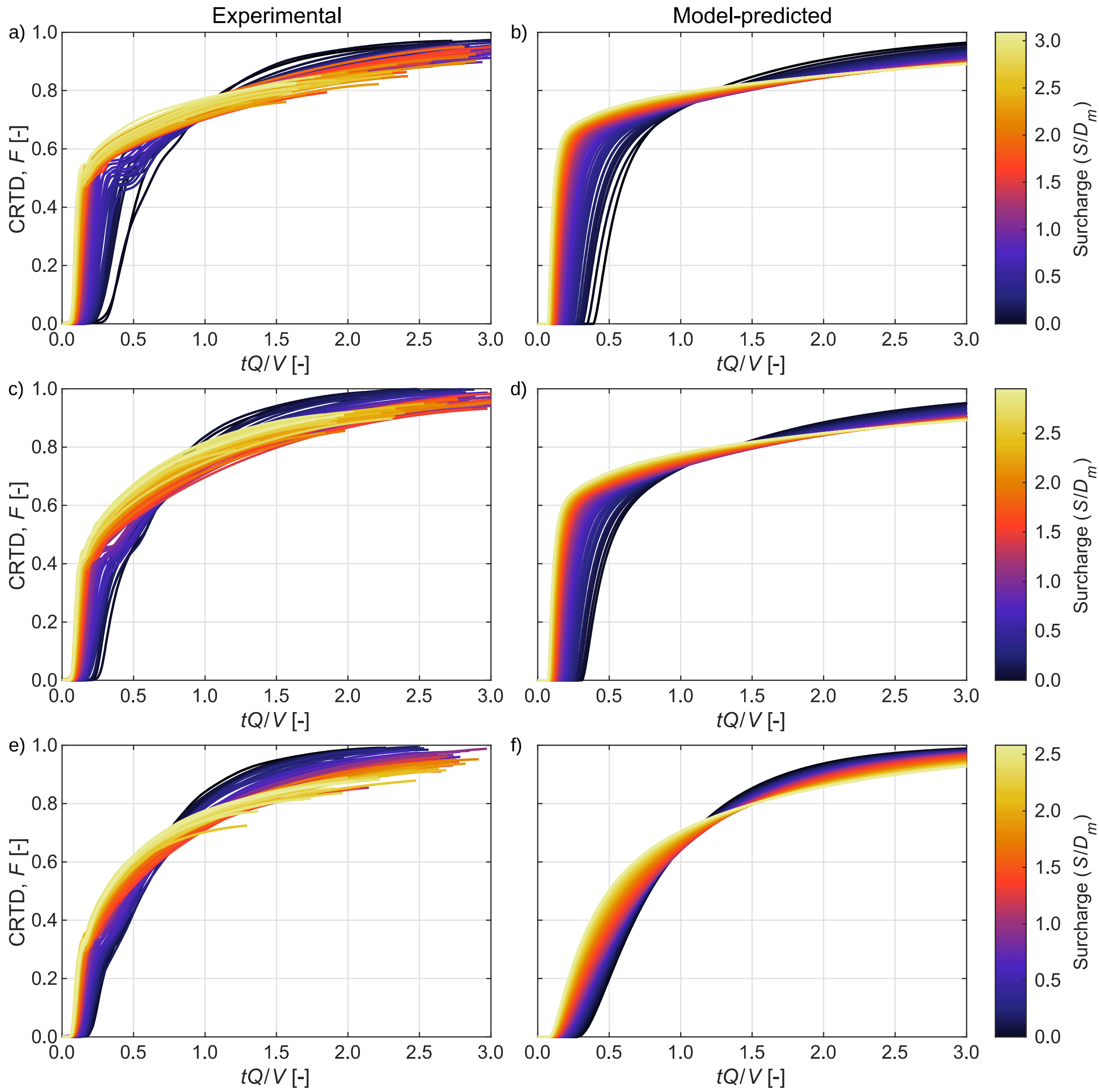

Fig. S2. Comparison of experimental deconvolved CRTDs (left) with new compartmental model predicted CRTDs (right) for stepped a) and b) B/D_p = 0.5, c) and d) B/D_p = 1.0, and e) and f) B/D_p = 2.0 manholes

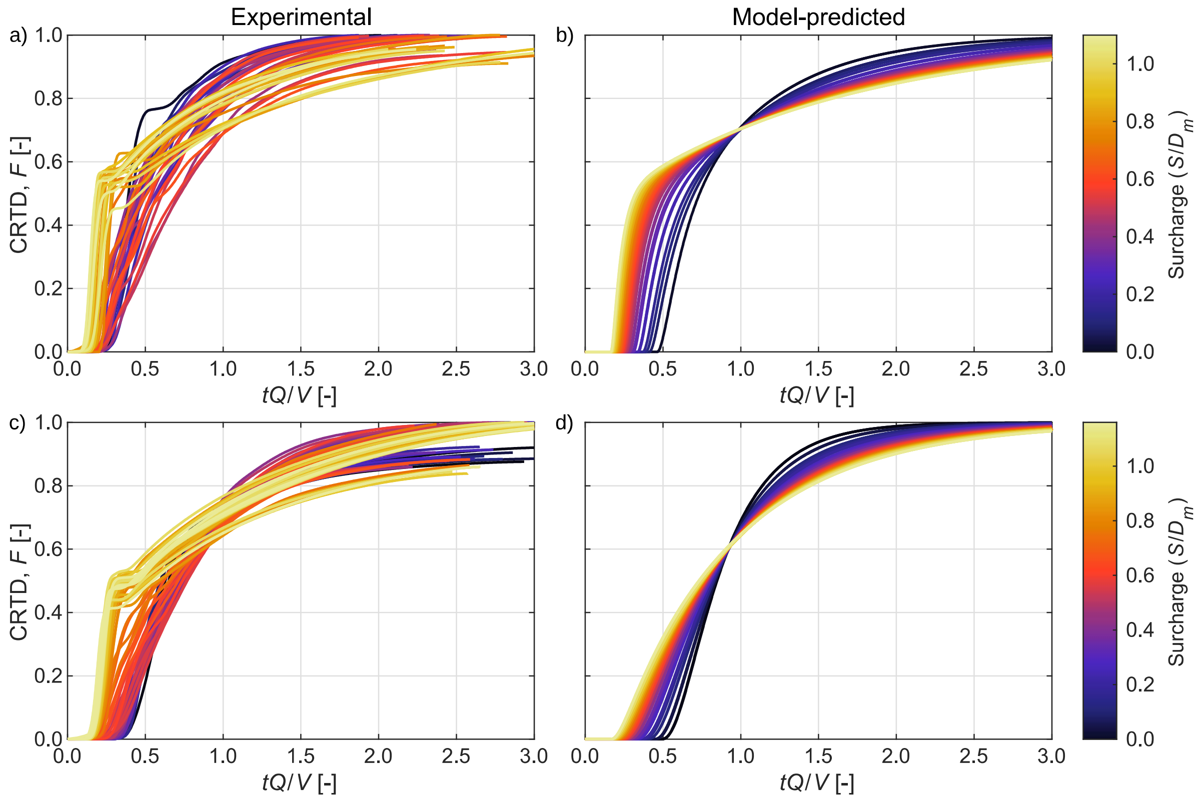

Fig. S3. Comparison of experimental deconvolved CRTDs (left) with new compartmental model predicted CRTDs (right) for angled a) and b) 30° and c) and d) 60° outlet manholes, CRTDs groups separated by $S/D_m \approx 0.71$ and $S/D_m \approx 0.78$ in a) and b) respectively